

Article

# Incorporation of Bioactive Glasses Containing Mg, Sr, and Zn in Electrospun PCL Fibers by Using Benign Solvents

Rachele Sergi <sup>1</sup>, Valeria Cannillo <sup>1</sup> , Aldo R. Boccaccini <sup>2</sup>  and Liliana Liverani <sup>2,\*</sup> 

<sup>1</sup> Dipartimento di Ingegneria Enzo Ferrari, Università degli Studi di Modena e Reggio Emilia, Via P. Vivarelli 10, 41125 Modena, Italy; rachele.sergi@unimore.it (R.S.); valeria.cannillo@unimore.it (V.C.)

<sup>2</sup> Department of Materials Science and Engineering, Institute of Biomaterials, University of Erlangen-Nuremberg, Cauerstr. 6, 91058 Erlangen, Germany; aldo.boccaccini@fau.de

\* Correspondence: liliana.liverani@fau.de; Tel.: +49-(0)9131-85-28603

Received: 4 July 2020; Accepted: 7 August 2020; Published: 10 August 2020



**Abstract:** Poly( $\epsilon$ -caprolactone) (PCL) and PCL/bioactive glass composite fiber mats were produced by electrospinning technique. To improve cell adhesion and proliferation (i) 45S5, (ii) a bioactive glass containing strontium and magnesium oxides, and (iii) a bioactive glass containing zinc oxide were separately added to the starting PCL solution before electrospinning. A good incorporation of bioactive glass particles in PCL electrospun mats was confirmed by SEM and FTIR analyses. Bioactivity was evaluated by immersion of PCL mats and PCL/bioactive glass electrospun fiber mats in simulated body fluid (SBF). Bone murine stromal cells (ST-2) were employed in WST-8 assay to assess cell viability, cell morphology, and proliferation. The results showed that the presence of bioactive glass particles in the fibers enhances cell adhesion and proliferation compared to neat PCL mats. Furthermore, PCL/bioactive glass electrospun mats showed higher wound-healing rate (measured as cell migration rate) in vitro compared to neat PCL electrospun mats. Therefore, the characteristics of the PCL matrix combined with biological properties of bioactive glasses make PCL/bioactive glass composite ideal candidate for biomedical application.

**Keywords:** PCL; bioactive glass; composite; electrospinning; wound healing

## 1. Introduction

Electrospinning is a widely used technique based on a starting polymeric solution and high electric field between two electrodes to fabricate nano- and micro- fibers for biomedical applications. Nanosized fibers mimicking the original structure of extracellular matrix (ECM) [1] can be fabricated by electrospinning technique. The features of samples are affected by (i) solution parameters (i.e., rheological properties, type of solvent(s), etc.), (ii) process parameters, and (iii) environmental parameters [1–4]. Among them, the selection of a proper solvent system plays a crucial role on the features of samples [5,6]. Recently, the standard solvents used for the electrospinning process, which are toxic, such as chloroform, dichloromethane, hexafluoro-2-propanol, dimethylformamide, methanol, or a mixture of them, have been increasingly substituted by less harmful solvents such as acetic acid, formic acid or acetone [7–9], which have been defined as benign solvents [10], highlighting the important properties related to prevention of biopolymer denaturation and presence of traces of toxic solvents on the fibers, as well as having a positive environmental impact.

Poly( $\epsilon$ -caprolactone) (PCL) has been widely used in combination with benign solvents (acetic acid or formic acid or acetone) to develop the starting polymeric solution for the production of electrospun mats [7–10]. PCL is widely investigated for biomedical applications because of its biocompatibility

and biodegradability [11–13] and is approved by the Food and Drug Administration (FDA) for clinical use. However, PCL bioactivity can be enhanced by the addition of bioactive biomaterials such as bioactive glasses (BGs). Generally, bioactive glasses have shown high bioactivity and high interaction with hard and soft tissues [14,15]. In this work, 45S5 BG (composition 45 wt% SiO<sub>2</sub>, 24.5 wt% CaO, 24.5 wt% Na<sub>2</sub>O, and 6.0 wt% P<sub>2</sub>O<sub>5</sub>) [16], Sr- and Mg-substituted bioactive glass (BGMS10 [17–23]), and Zn-substituted bioactive glass (BGMS\_2Zn [24]) were incorporated in PCL fibers by electrospinning technique. BGMS10 was designed starting from the composition of 45S5 by adding SrO and MgO; subsequently, ZnO was added to the BGMS10 composition to produce a Zn-substituted bioactive glass labelled as BGMS\_2Zn [24]. The incorporation of different ions into bioactive glass compositions aims to impart specific biological functionalities and to enhance the therapeutic behavior [25–28]. In particular, Sr has been shown to enhance osteogenic differentiation, to stimulate osteoblast differentiation [29] and bone formation [30–33] as well as angiogenesis and cell proliferation [34–36]. Furthermore, Sr, because of its anabolic and anti-resorptive effect on bone, is already in use as strontium ranelate in the treatment of osteoporosis [37]. Mg, which is the 4th most abundant cation in the human body, not only stimulates stem cells proliferation and differentiation but it plays a pivotal role in bone metabolism by enhancing ALP activity [38]. Furthermore, Mg can be useful for bone regeneration [39,40]. Therefore, it is expected that PCL fibers containing BGMS10 and BGMS\_2Zn particles will release Sr and Mg showing enhanced cell adhesion and proliferation in in vitro tests. In addition, it is expected that PCL fibers containing BGMS\_2Zn particles will also release Zn ions. Zn is not only essential for cell growth and proliferation, but it also takes part in enzyme production, replication of DNA, and growth factors (GFs) [41–43]. Furthermore, Zn ions have shown antimicrobial properties [44–46]. Therefore, the incorporation in PCL fibers of such ion-doped BGs aims to enhance bioactivity, cell proliferation, and angiogenesis as well [47–50]. Because of the capacity of bioactive glasses to stimulate both hard and soft tissues, PCL/bioactive glass composite fiber mats could represent the starting materials for wound-healing devices. The use of composites combines the properties of the organic matrix with the reinforcement of the inorganic phase embedded into the fibers which could be suitable for the fabrication of healing devices with suitable mechanical and biological performance [8].

## 2. Materials and Methods

### 2.1. Bioactive Glasses Preparation

BGMS10 and BGMS\_2Zn were manufactured by the conventional melt-quenching route as reported in the literature [51–53]. In brief, the commercial raw powders (SiO<sub>2</sub>, Ca<sub>3</sub>(PO<sub>4</sub>)<sub>2</sub>, CaCO<sub>3</sub>, Na<sub>2</sub>CO<sub>3</sub>, K<sub>2</sub>CO<sub>3</sub>, MgCO<sub>3</sub>, SrCO<sub>3</sub>, ZnO, from Carlo Erba Reagenti, Cornaredo, Italy) were mixed for 3 h in a laboratory shaker (M63a4-Motori Elettrici Carpanelli, Bologna, Italy) and then melted in a platinum crucible (in air). The thermal cycle was the following: from room temperature to 1100 °C at 10 °C/min; a decarbonation step at 1100 °C for 2 h; from 1100 °C to 1450 °C at 10 °C/min followed by keeping 1450 °C constant for 45 min. The fused glass was rapidly quenched in room-temperature water to have a frit, which was dried at 110 °C for 12 h. The frit of each glass composition was then milled to obtain bioactive glass powders with final grain size to achieve an effective incorporation inside PCL fibers. The average particle size of the different powders was calculated using ImageJ (NIH, Bethesda, MD, USA) [54] from the SEM micrographs reported in Figure 1 and resulted in the following values: 2.4 μm for 45S5, 2.3 μm for BGMS10 and 3.2 μm for BGMS\_2Zn.

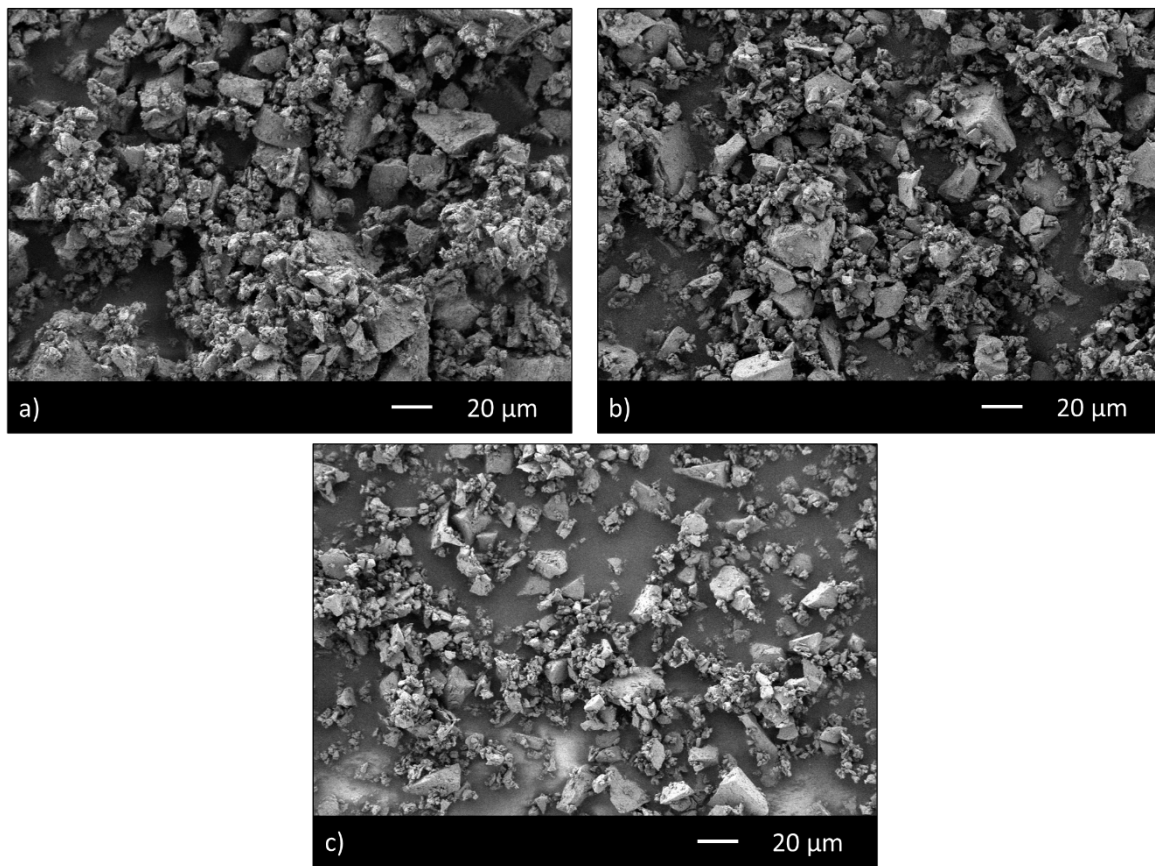


**Figure 1.** SEM analysis of bioactive glass particles after milling before electrospinning: 45S5 (a), BGMS10 (b), and BGMS\_2Zn (c).

Subsequently, bioactive glass powders were added to the starting polymeric solution before electrospinning. The composition of the BGs investigated is shown in Table 1.

**Table 1.** Summary of bioactive glasses (BGs) compositions reported in wt%.

BG Label	SiO <sub>2</sub>	CaO	Na <sub>2</sub> O	K <sub>2</sub> O	P <sub>2</sub> O <sub>5</sub>	MgO	SrO	ZnO
45S5 [16]	45	24.5	24.5	-	6	-	-	-
BGMS10 [17–23]	44	22.3	2.2	3.4	5.7	6.3	16.1	-
BGMS_2Zn [24]	41.1	20.8	2	3.1	11	5	15	2

## 2.2. Solution Preparation

Electrospun mats were obtained from PCL (80 kDa, Sigma Aldrich, Munich, Germany) solutions and acetic acid (AA, VWR, Darmstadt, Germany) was used as solvent. The solutions of PCL in acetic acid (20% *w/v*) were mixed overnight and then were ultrasonicated for 1 h before electrospinning. To produce the composite electrospun mats, 45S5, BGMS10, and BGMS\_2Zn were homogeneously dispersed (5 wt% respect to PCL) in the polymer solution and mixed for 10 min and subsequently immersed in ultrasonic bath for 1 min before electrospinning. The amount of bioactive glass was chosen at 5 wt% because previous studies demonstrated that adding only 5 wt% bioactive glass to PCL can already generate relevant *in vitro* and *in vivo* outcomes with respect to PCL only [55]. In particular, the focus of this work is the development of composite fibers with suitable properties for applications in soft tissue engineering, as widely reported [47–50] and it is not oriented to the osteogenic differentiation as reported in [55]. The composite electrospun mats were namely PCL, PCL\_45S5, PCL\_BG10, and PCL\_BGZn.

### 2.3. Electrospinning Process

The electrospinning parameters used (Table 2) have been previously optimized as reported elsewhere [8]. Briefly, the electrospinning parameters to fabricate PCL electrospun mats were: (i) 15 kV voltage; (ii) 11 cm needle-target distance; (iii) 0.4 mL/h flow rate with a needle diameter of 0.8 mm. The process was executed with a commercial device equipped with a climate control chamber EC-CLI (IME Medical Electrospinning) and the environmental parameters as temperature (T) and relative humidity (RH%) were set at 25 °C and 40%, respectively. On the other hand, to fabricate the PCL\_45S5, PCL\_BG10 and PCL\_BGZn composite electrospun mats the parameters of electrospinning were the same used for neat PCL except for the flow rate which was increased from 0.4 mL/h to 0.6 mL/h.

**Table 2.** Summary of parameters used for the different solutions during electrospinning process.

Sample Name	Solution Concentration (%w/v)	Solvent(s)	kV	Distance Tip-Target (cm)	Needle Diameter (mm)	Flow Rate (mL/h)	T (°C)	Relative Humidity (% RH)
PCL	20	Acetic acid	15	11	0.8	0.4	25	40
PCL_45S5, PCL_BG10, PCL_BGZn	20	Acetic acid	15	11	0.8	0.6	25	40

### 2.4. Microstructural Characterization

The morphology of samples was investigated by means of scanning electron microscopy (SEM) analysis (FE-SEM-EDS (Auriga Base, Zeiss, Jena, Germany)). Sputter Coater (Q150T, Quorum Technologies, Darmstadt, Germany) was used to sputter with gold the samples before SEM analysis. ImageJ (NIH, Bethesda, MD, USA) was used to calculate fibers average diameters of 50 fibers from each sample [54]. SEM analysis was performed before and after immersion in simulated body fluid (SBF) solution (see Section 2.6); the eventual formation of hydroxy-carbonate apatite (HCA) layer on samples' surface was investigated by means of SEM. Furthermore, FTIR spectra before and after immersion in SBF were obtained using the FTIR spectrometer (Shimadzu, IRAffinity-1S, Fourier Transform infrared spectrophotometer, Duisburg, Germany). For the analysis, 40 spectral scans at resolution of 4 cm<sup>-1</sup> were repeated over the wavenumber range 4000–400 cm<sup>-1</sup>.

### 2.5. Mechanical Testing, Contact Angle, and Thermal Behavior

The mechanical properties of the electrospun fibers were investigated by means of uniaxial tensile test at room temperature (5960 Dual Column Tabletop Testing System, Instron®, Darmstadt, Germany) by fixing electrospun samples in a paper frame, following the protocol reported in [9]. Five samples for each electrospun mat were tested. Furthermore, contact angle measurements were performed by releasing 3 µL of distilled H<sub>2</sub>O (Krüss DSA30, Hamburg, Germany) to assess the wettability of electrospun fibers. Thermogravimetric analysis and differential thermal analysis (TG/DTA) (Netzsch Differential Thermal Analyzer STA 429 CD, NETZSCH-Gerätebau GmbH, Selb, Germany) were employed to ascertain the incorporation of bioactive glass particle considering the residual amount of mass after PCL decomposition. Thermal decomposition analysis was executed in static air atmosphere on 30 mg of samples heated from 25 °C to 800 °C at 10 °C/min. The tests were performed in static air atmosphere.

### 2.6. In Vitro Bioactivity

The samples were immersed in SBF solution to assess their in vitro bioactivity, which is defined as the ability to form hydroxycarbonate apatite once immersed in physiological fluids. The SBF solution was prepared following the protocol developed by Kokubo et al. [56,57]. The ratio between the surface of samples and the SBF volume was calculated according to [57]. Before soaking in SBF, the samples were fixed on scaffold holders (Scaffdex, Sigma Aldrich). The samples (PCL, PCL\_45S5, PCL\_BG10

and PCL\_BGZn) were kept in self-stand Falcon tubes at 37 °C in an incubator on an oscillating tray for 1, 7, 14, and 21 days. The SBF solution was refreshed every 3 days and the pH was measured every day. At each time point, the samples were immediately washed with distilled H<sub>2</sub>O and dried at room temperature. The eventual HCA layer formation on samples' surface was studied by SEM and FTIR spectroscopy.

## 2.7. Biological Tests

### 2.7.1. Bone Murine Stromal Cells ST-2

Bone murine stromal cells ST-2 (Leibniz-Institut DSMZ—German Collection of Microorganisms and Cell Cultures GmbH, Braunschweig, Germany) were used to investigate cell viability, cell morphology, and proliferation. ST-2 cell line was selected because it showed osteoblast [58], chondrocyte [59], and adipocyte differentiation [60], confirming to be appropriate for preliminary studies for both soft and hard tissue engineering applications. Before the seeding, ST-2 cells were cultured in RPMI 1640 medium (Thermo Fisher Scientific, Erlangen, Germany), supplemented with 10% fetal bovine serum (Lonza) and 1% penicillin/streptomycin (Lonza) and incubated at 37 °C with 5% CO<sub>2</sub>.

### 2.7.2. WST-8 Assay

Sample holders (Scaffdex, Cellcrown™, Sigma Aldrich, Munich, Germany) were used to fix all the electrospun mats, the samples with the inserts were put in 24-multiwell plate and disinfected by exposure to UV light for 1 h, before cell seeding. An inoculum ratio of  $1.5 \times 10^5$  cells/mL with a drop of 100 µL per sample was used for seeding cells. After 15 min of incubation at 37 °C, 1 mL of RPMI medium was added to each well. WST-8 assay (CKK-8, Sigma) was performed 1 day and 7 days after the seeding in triplicate on all samples, according to [61]. Cell morphology was investigated 7 days after seeding by staining with rhodamine phalloidin, and DAPI (Thermo Fisher Scientific). Rhodamine phalloidin solution (8 µL/mL) and DAPI solution (1 µL/mL) were employed for the staining, according to the protocol previously described in [10]. All samples were then investigated by a fluorescence microscope (Axio Scope A1, Zeiss, Jena, Germany).

### 2.7.3. Scratch Test

*In vitro* scratch test is based on the observation of a gap (i.e., the “scratch”) on a confluent monolayer of cells until the contact between cells is established again [62,63]. Images are taken immediately after the creation of the scratch and at regular intervals to investigate cell migration. At the end, images collected at each time point are compared to ascertain the rate of cells migration.

Mouse embryonic fibroblast cells (NIH 3T3) were seeded in 24-multi-well and incubated at 37 °C to allow the creation of a confluent monolayer. Cells were cultured in Dulbecco's modified Eagle's medium (DMEM) containing L-glutamine 2 mM, 1 mM sodium pyruvate, 10 mg/mL penicillin/streptomycin, and 10% (*v/v*) FBS (fetal bovine serum, Invitrogen, Thermo Fisher Scientific, Rodano, Italy). The type of cells and the size of the multi-well influence the number of cells required to create a confluent monolayer. To produce the scratch, by scraping the confluent monolayer of cells, a 200-µL pipet tip was used. Then, cells were immediately washed with 500 µL of PBS and in each well 500 µL of medium (DMEM) and 500 µL of the eluates of electrospun fibers (PCL, PCL\_45S5, PCL\_BG10 and PCL\_BGZn) were added. Eluates were prepared by soaking samples (3 cm<sup>2</sup>/mL surface of sample/liquid volume) in DMEM and incubated at 37 °C for 72 h. Then, samples' eluates were filtered before their usage with cells. To acquire the same area of the scratch during image acquisition, a visible mark was created. Images were taken immediately after the creation of the scratch on confluent monolayer (i.e., time 0) before incubating the multi-well at 37 °C until the next time points. Images were acquired at three time points: at time 0, time 1 (24 h after the scratch), and time 2 (48 h after the scratch). For each image,

ImageJ (NIH, Bethesda, MD, USA) [54] was used to measure the area of the gap between the edges of the scratch. The cell migration rate was calculated as follows according to [64]:

$$\text{Cell migration rate (\%)} = \frac{A0 - A1}{A0} \times 100 \quad (1)$$

where  $A0$  is the area of the gap at time 0 and the  $A1$  is the area of the gap at time  $X$  where in this case  $X$  is either 24 h or 48 h.

#### 2.7.4. Statistical Analysis

ANOVA one-way analysis was performed to evaluate the results of cell viability and mechanical testing. A  $p$ -value  $< 0.05$  was considered statistically significant.

### 3. Results and Discussion

#### 3.1. Microstructural Characterization

SEM analysis of PCL, PCL\_45S5, PCL\_BG10, and PCL\_BGZn (Figure 2a–d) showed a homogeneous fiber diameter distribution. Some bioactive glass particles embedded in PCL matrix are observed in the insets in Figure 2b–d. The average fiber diameter was calculated by ImageJ [54] to verify the influence of bioactive glass particles on fiber diameter. The average fiber diameter was  $1.3 \pm 0.4 \mu\text{m}$  for neat PCL; while  $1.0 \pm 0.7 \mu\text{m}$ ,  $1.2 \pm 0.6 \mu\text{m}$ , and  $1.1 \pm 0.7 \mu\text{m}$  were the average values for PCL\_45S5, PCL\_BG10, and PCL\_BGZn fibers, respectively. These results demonstrate that bioactive glass particles did not influence the morphology of fibers in terms of average fiber diameter.

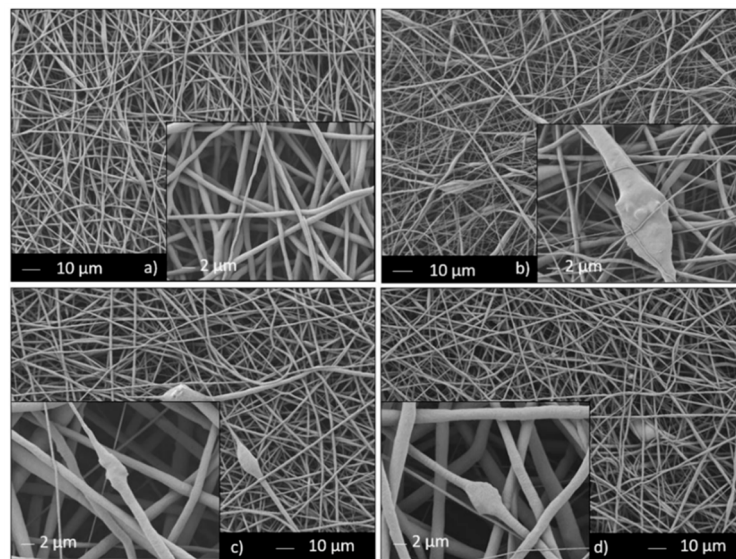


**Figure 2.** SEM analysis of electrospun mats: PCL (a), PCL\_45S5 (b), PCL\_BG10 (c), and PCL\_BGZn (d).

Furthermore, to verify the presence of bioactive glass particles in the fibers, the composite electrospun mats were characterized by EDX (Figure 3b–d). Although EDX analysis is not a quantitative analysis, elements present in bioactive glasses such as Si, Ca, Na were detected confirming the incorporation of bioactive glass particles in PCL matrix. C element from the PCL matrix was also detected.

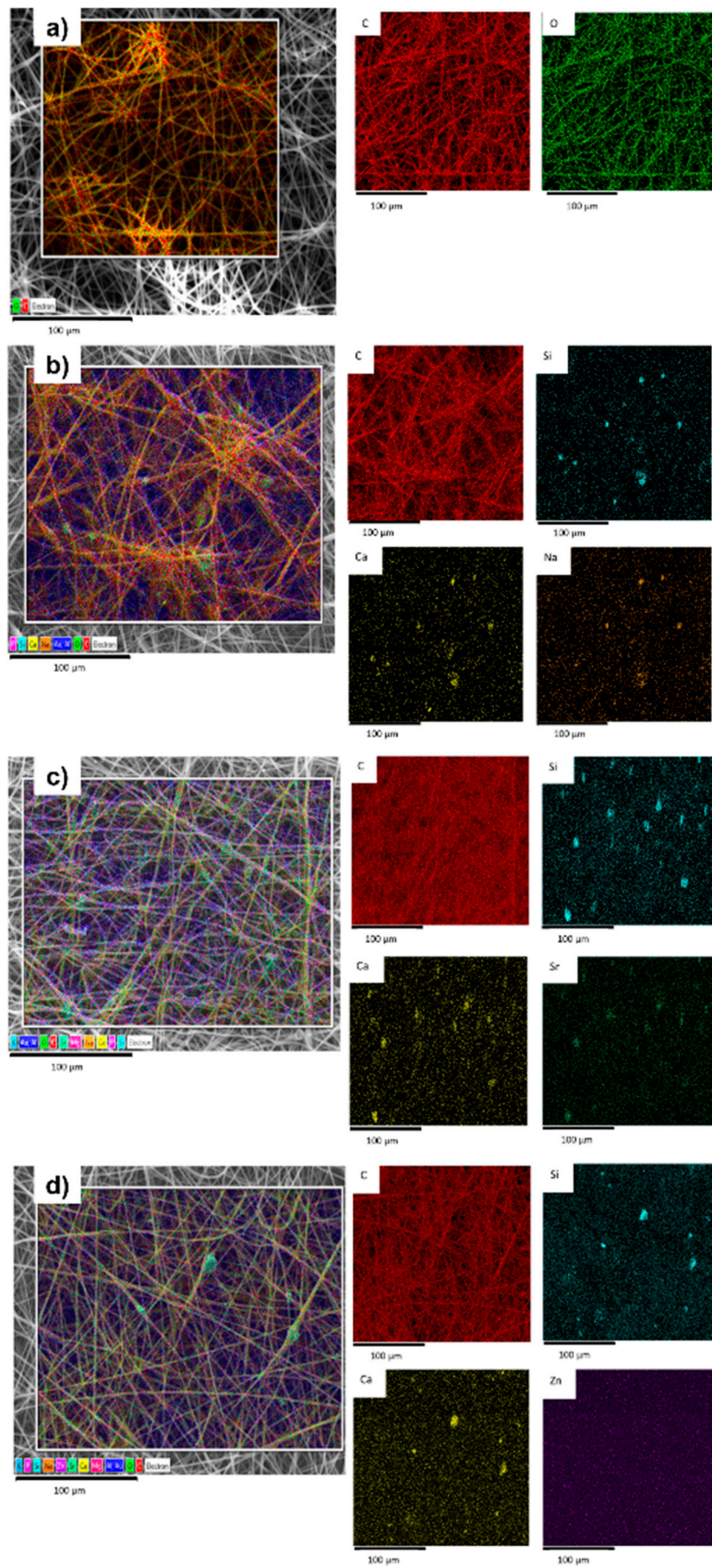


**Figure 3.** EDX mapping of electrospun PCL (a) and composites PCL\_45S5 (b), PCL\_BG10 (c), PCL\_BGZn (d) at d0 (before immersion in simulated body fluid (SBF)).

FTIR analysis was performed to detect the characteristic bands of bioactive glass particles embedded in PCL fibers. Figure 4 showed the characteristic bands of PCL: (i) two bands at 2942 and 2867  $\text{cm}^{-1}$  ascribed to  $\text{CH}_2$  asymmetric and symmetric stretching [65]; (ii) a band at 1722  $\text{cm}^{-1}$  correlated to carbonyl stretching [66]; (iii) a band at 1294  $\text{cm}^{-1}$  related to the C-O and C-C stretching [67]; and (iv) two bands at 1241 and 1164  $\text{cm}^{-1}$  ascribed to the asymmetric and symmetric C-O-C stretching, respectively [61,65]. Unfortunately, the bands ascribed to stretching and bending of functional groups (i.e., Si-O-Si) of bioactive glass particles were not detected, since they overlap with the above mentioned bands. Such overlapping is highlighted in Figure 4; the different shape of the characteristic peak at 1164  $\text{cm}^{-1}$  of PCL in PCL/bioactive glass composites can be ascribed to the overlapping of Si-O-Si group of bioactive glasses [68]. This could also be related to the low amount of bioactive glass particles added to PCL starting solution (5%wt with respect to PCL).

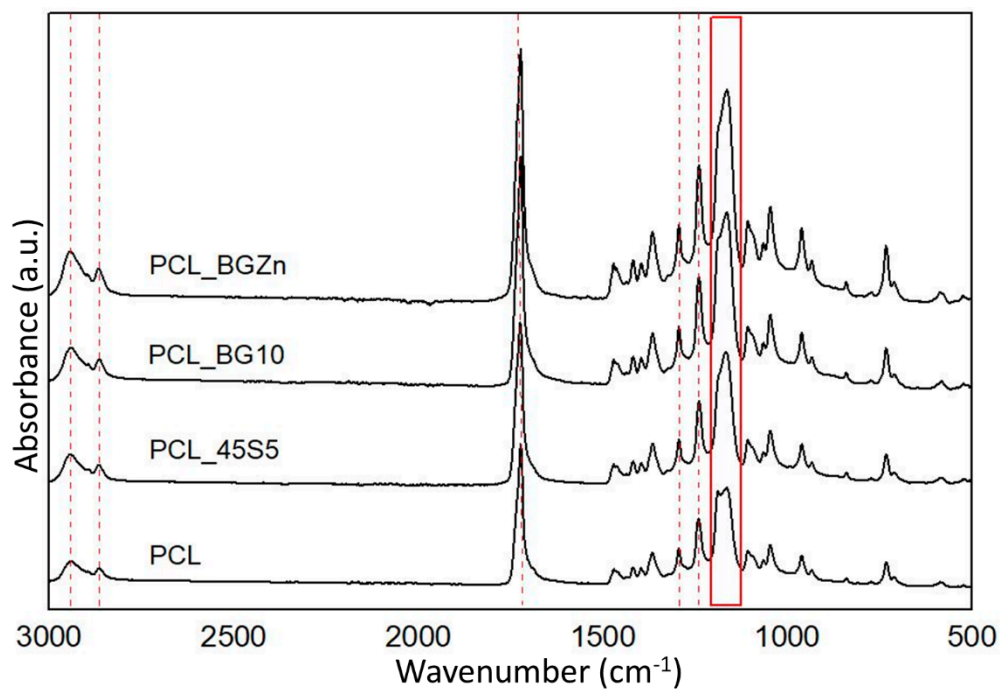


**Figure 4.** FTIR spectra of PCL, PCL\_45S5, PCL\_BG10, and PCL\_BGZn electrospun mats before immersion in SBF solution. The indicated peaks are discussed in the text.

### 3.2. Mechanical Testing, Thermal Characterization, and Contact Angle Measurement

Electrospun mats fixed in a paper frame were mounted in the tensile tester and investigated to determine the Young's modulus and strain at break. A significantly lower value ( $p < 0.05$ ) of tensile strain (%) could be observed for PCL\_45S5, PCL\_BG10, and PCL\_BGZn compared to the value of PCL electrospun mats (Table 3).

**Table 3.** Tensile strain, Young's modulus and contact angle values for PCL, PCL\_45S5, PCL\_BG10, and PCL\_BGZn.

Sample Name	Tensile Strain (%)	Young's Modulus (MPa)	Contact Angle (°)
PCL	496 ± 20	12 ± 1	104 ± 17
PCL_45S5	95 ± 1	4.5 ± 0.9	105 ± 11
PCL_BG10	221 ± 14	12 ± 3	96 ± 2
PCL_BGZn	113 ± 18	12 ± 2	104 ± 19

In the same table the Young's modulus is reported. Generally, the decrease of the value of tensile strain (%) could be correlated with the incorporation of bioactive glass particles in PCL matrix. Bioactive glass particles weaken the entire composite electrospun mat in terms of displacement because the particles act as rigid inclusion inside PCL matrix, as already reported in [9].

Furthermore, the contact angle was measured as it provides unique insight into how the surface will interact with the external world. A drop of liquid on a solid surface represents a powerful but simple method to investigate the properties of the surface [69]. A change in the contact angle of PCL electrospun mats and composite (PCL\_45S5, PCL\_BG10, and PCL\_BGZn) electrospun mats could be an indicator of successful surface modification. However, contact angle also relies on both the porosity and roughness of the surface of electrospun mats. Generally, when a drop of water is placed on electrospun fibers only a fraction of water encounters the fibers, decreasing the liquid–solid interactions and increasing the liquid–air interactions. This leads to higher contact angles compared to that measured for smooth surfaces, like films [70]. Moreover, when measuring contact angles of electrospun mats it is difficult to estimate the circular part of the drop profile with the surface when it is irregular. However, as expected, the results showed hydrophobic behavior for all samples (Table 3). The bioactive glass particles incorporated in the PCL matrix seems not to affect the hydrophobic behavior of PCL electrospun mats because the values of contact angle were comparable for all samples.

PCL decomposition was investigated by TG/DTA analyses (Figure 5). Generally, PCL shows single stage thermal degradation [71]. PCL decomposed completely in the region 350 °C to 420 °C (Figure 5) where a significant weight loss is recorded [72]. Each exothermic peak at around 450 °C represent the  $T_{max}$  (i.e., the maximum degradation rate) [67]. The residual weight in PCL\_45S5, PCL\_BG10, and PCL\_BGZn was due to the presence of bioactive glass particles embedded in the PCL fibers. For PCL\_45S5 the amount was similar to the initial amount added in the polymeric solution, while for PCL\_BG10 and PCL\_BGZn it was less than 5% wt (the residual weight was 2.25 wt% of BGMS10 and 3.33 wt% of BGMS\_2Zn). In fact, the mass loss after heating was 95.25% for PCL\_45S5, 97.75% for PCL\_BG10, and 96.67% for PCL\_BGZn.

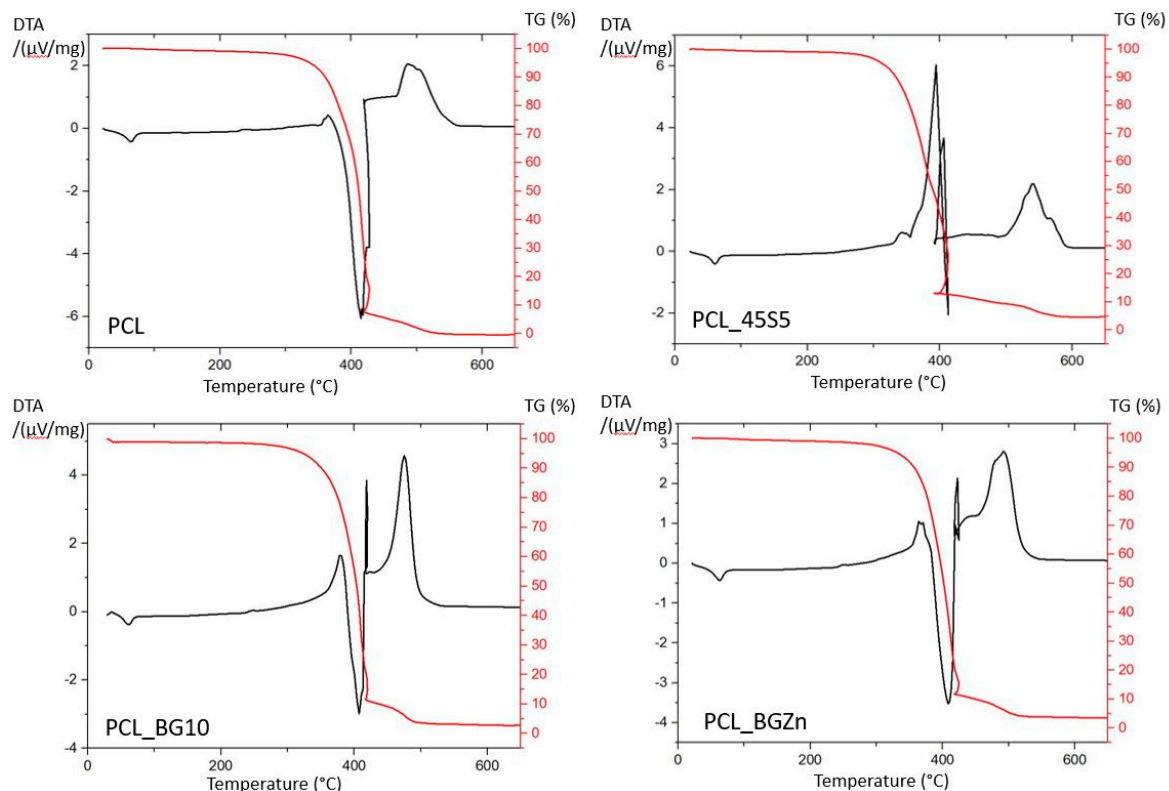


**Figure 5.** TG/DTA analyses of PCL, PCL\_45S5, PCL\_BG10, and PCL\_BGZn.

### 3.3. In Vitro Bioactivity Investigation

SEM and EDX analyses 7, 14, and 21 days after immersion in SBF on PCL\_45S5, PCL\_BG10, and PCL\_BGZn were performed. In case of wound dressing applications, mineralization is not of pivotal importance as it is for biomaterials used mainly for bone regeneration. However, its role and relevance in wound-healing applications is still a matter of discussion [73]. For this reason, considering that in vitro bioactivity tests have been commonly performed also on films or hydrogels developed for wound-healing applications [74,75], the same test was performed on the developed PCL composite fibers. FTIR spectra after soaking in SBF solution showed the bands that correspond to HCA layer. At around  $600\text{ cm}^{-1}$  the P-O bending vibration (Figure 6a–d) was detected [76]. PCL\_45S5 spectra (Figure 6b) showed a broad band at around  $1046\text{ cm}^{-1}$  which could be the overlap of PCL peak ( $1046\text{ cm}^{-1}$ ) and the P-O asymmetric stretching vibration at around  $1030\text{ cm}^{-1}$  correlated to the presence of HCA on electrospun mats [77]. The P-O asymmetric stretching vibration at around  $1030\text{ cm}^{-1}$  in addition to P-O bending vibration at around  $600\text{ cm}^{-1}$  was detected for PCL\_45S5 1 day after immersion in SBF. While P-O asymmetric stretching vibration was detected 7 days after immersion for PCL\_BG10 and PCL\_BGZn samples (Figure 6c,d). Furthermore, FTIR spectra at 14 days and 21 days after immersion in SBF, showed P-O bending vibration but it was difficult to detect the broader peaks at around  $1040\text{ cm}^{-1}$ . The lower bioactivity of PCL\_BGZn could be ascribed to the lower bioactivity of BGMS\_2Zn bioactive glass compared to 45S5. The presence of a relatively low amount of HCA indicates a slow ion exchange with the surrounding solution. It is reported that Zn ions hinder ions involved in the exchange with the surrounding environment delaying HCA precipitation [78]. ZnO could behave both as a network modifier and as an intermediate oxide. It is supposed that ZnO behaves as a network modifier because it replaces CaO [79], forming tetrahedral species ( $\text{ZnO}_4^{2-}$ ) which required Ca ions for charge balancing. This behavior decreases glass bioactivity by reducing glass dissolution [80] because cations from silica network are removed. Additionally, by increasing the amount of Zn ions, a decrease in the releasing of alkaline earth ions (i.e.,  $\text{Ca}^{2+}$ ,  $\text{Mg}^{2+}$ ) and alkali ions (i.e.,  $\text{Na}^+$ ,  $\text{K}^+$ ) occurs [81–83]. This behavior is verified by the low oscillation of pH during soaking time which leads to a low interchange between alkaline, alkali ions, and  $\text{H}_3\text{O}^+$  ions of the surrounding solution, as outlined in previous studies [81–83]. Therefore, Zn ions decrease the degradation of bioactive glass and consequently the formation of HCA on PCL\_BGZn was delayed.

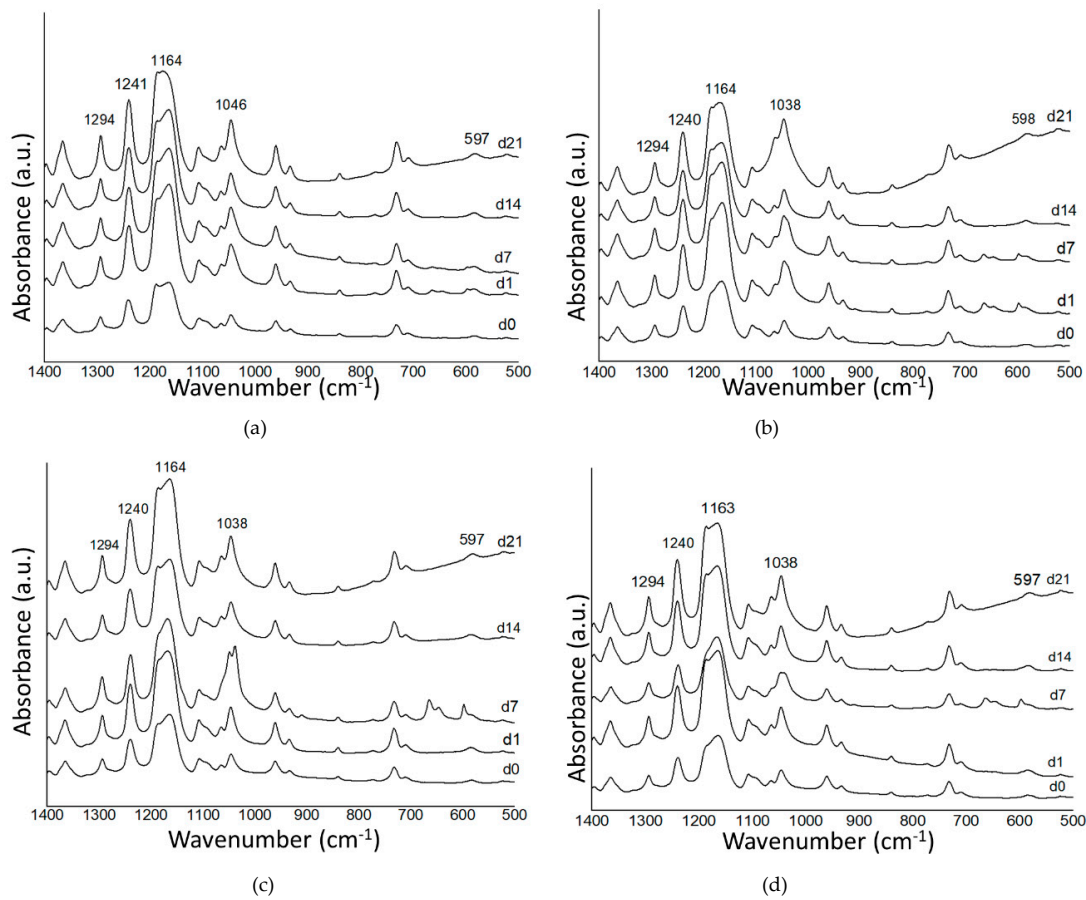


**Figure 6.** FTIR spectra before immersion (0d) in SBF and 1, 7, 14, 21 days after immersion in SBF for: PCL (a); PCL\_45S5 (b); PCL\_BG10 (c); and PCL\_BGZn (d). Relevant indicated peaks are discussed in the text.

### 3.4. Biological Investigation

#### 3.4.1. WST-8 Assay

WST-8 results (Figure 7) show that 1 day after seeding PCL\_45S5 has lower OD values compared to neat PCL electrospun mats used as control; on the other hand, PCL\_BGZn and PCL\_BG10 showed comparable OD values.

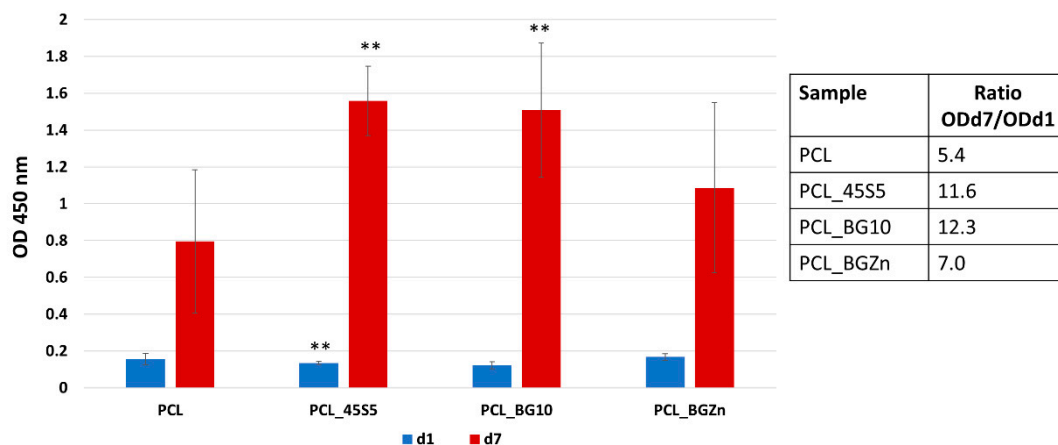


**Figure 7.** WST-8 analysis: graph of OD at 450 nm for all electrospun mats 1 day and 7 days after seeding. \*\*  $p < 0.05$  (one-way ANOVA) and a table reporting the ratio ODD7/ODD1.

7 days after seeding, PCL\_45S5 and PCL\_BG10 showed higher OD values compared to PCL, while PCL\_BGZn had a comparable value (Figure 7). To highlight the effect of the presence of BGs on cell viability the ratio between the OD at 7 days (ODd7) and the OD measured after 1 day (ODd1) from the seeding was calculated for all samples and is shown in Figure 7. It is relevant to notice that this value is higher for all composites mats with respect to neat PCL while PCL\_BG10 shows the highest value. This behavior could be due to the ions released by bioactive glass particles. In fact, it is known that bioactive glasses influence cell proliferation with an increase in the level of differentiation markers such as ALP, osteocalcin, and osteopontin and they improve osteogenesis by controlling genes involved in the cell cycle toward mature osteoblasts [84]. Additionally, BGs release ions such as Si, Ca, Na, P that can activate the osteogenesis related signaling pathway [85]. Therefore, the incorporation of bioactive glass particles enhances cell viability 7 days after seeding compared to PCL electrospun fiber mats. Additionally, 45S5 and BGMS10 seem to have higher effect than BGMS\_2Zn. Although PCL\_BGZn showed OD values higher than those of PCL, it showed lower cell viability compared to PCL\_45S5 and PCL\_BG10 samples. This behavior is probably due to Zn ions released that could become toxic in an in vitro environment characterized by the absence of fluid exchange as is the case inside the human body [86,87].

The morphology of cells was investigated by means of fluorescence microscopy 7 days after seeding. The fluorescence staining corroborates the results obtained by WST-8 assay. All samples (Figure 8) showed cells in their characteristic shape spread on electrospun mats.

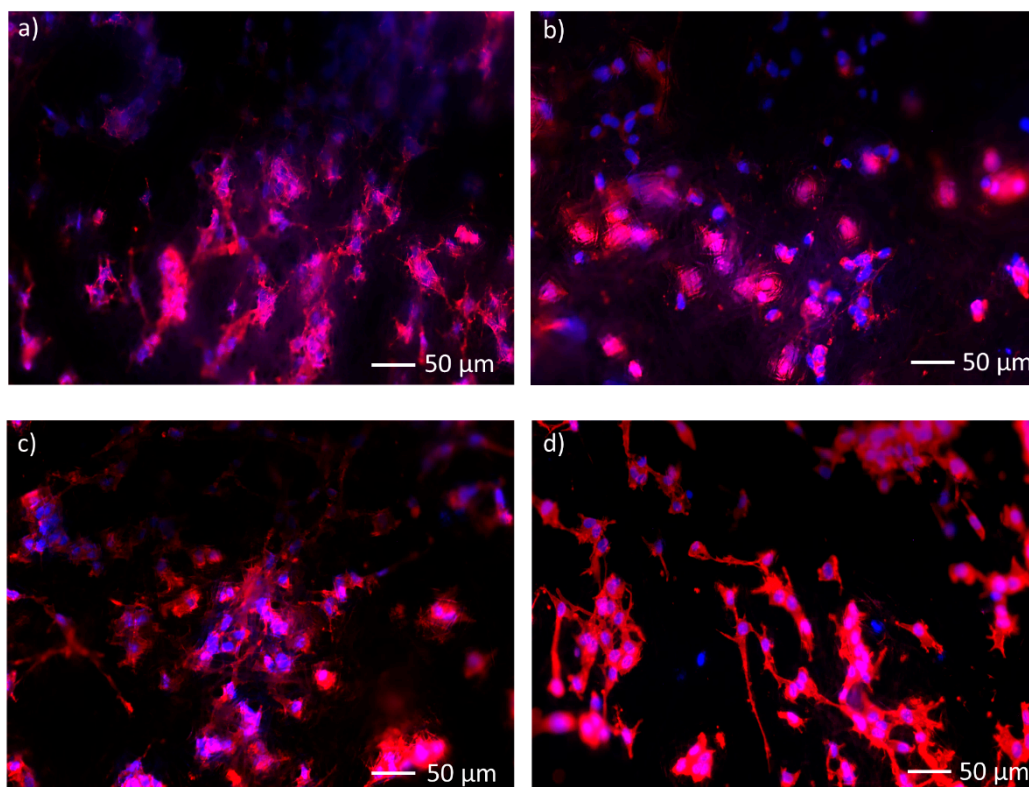


**Figure 8.** Fluorescence images of actin filaments (red) and cell nuclei (blue) for PCL (a), PCL\_45S5 (b), PCL\_BG10 (c), and PCL\_BGZn (d) 7 days after the seeding.

It is possible to observe that the cells seeded on PCL\_BG10 and PCL\_BGZn showed a more elongated morphology with respect to neat PCL and PCL\_45S5, suggesting that the presence of Mg and Sr could affect cell adhesion on the fibers [88–90].

### 3.4.2. Scratch Test

As mentioned, the *in vitro* scratch test is a cheap, easy, and well-developed method to measure cell migration *in vitro* [62,63]. The *in vitro* scratch test is useful to evaluate the migration of cells after the creation of a gap on confluent monolayer. Such test mimics cell migration *in vivo* and it is advantageous to assess through cell–cell interaction and cell interaction with ECM the regulation of cell migration [91]. Additionally, the scratch test uses inexpensive and common supplies found in most laboratories of cell culturing, thus, it is the simplest method to analyze the migration rate of cells *in vitro*.

To assess the effect PCL and PCL/bioactive glass composite electrospun mats on NIH 3T3 cells, the closure of the gap in monolayers of mouse embryonic fibroblast was investigated. The scratches in monolayers of cells were created by the tip of a 200- $\mu$ L pipette and the closure of such scratches was measured at 24 h and 48 h. At 24 h, a significant closure in terms of wound-healing rate (%) (measured as cell migration rate) was registered for PCL\_BG10 and PCL\_BGZn, compared to neat PCL and PCL\_45S5.

At 48 h, the cell migration rate (%) of PCL/bioactive glass composite electrospun mats was higher compared to that measured for neat PCL (Figure 9). 45S5, BGMS10, and BGMS\_2Zn influenced positively the closure of the scratch on the confluent mouse embryotic fibroblast monolayer. The reason could be ascribed to ions released by different BGs to stimulate specific signaling pathways promoting cellular response [92]. For instance, 45S5 release Ca and Si ions that contribute to the formation of HCA and are involved in specific signaling pathways [93,94]. It has been reported that Ca ions are involved in the regulation of Golgi, mitochondrial shuttling, and endosomal and vesicular fusion events etc., [95]; thus, Ca ions influence every aspect of cell life and death [96]. Additionally, Si ions showed a strong stimulatory effect on ALP activity [31]. Furthermore, Sr ions in BGMS10 and BGMS\_2Zn have been shown to significantly enhance the expression of ang-1 and VEGF compared to Si ions [31]. Additionally, PCL\_BGZn composite mats contain Zn ions that have been shown to stimulate protein synthesis and to enhance ALP activity as presented in [40]. Free intracellular Zn level influences signaling pathway and stability [97] by altering the affinity between ligand binding to receptor [98]. The intracellular zinc has shown to activate MAPK/ERK and Akt pathways which improve cell proliferation and migration [99]. Furthermore, the release of Zn into the cytoplasm seems to be ROS-induced. Key immune functions are activated by both the increase of ROS level and the Zn signal [100]. Therefore, the high wound-healing rate (%) of PCL/bioactive glass composite electrospun mats (Figure 9) could be attributed to the release of ions which have been shown to improve cell adhesion and proliferation by stimulating specific cellular responses.

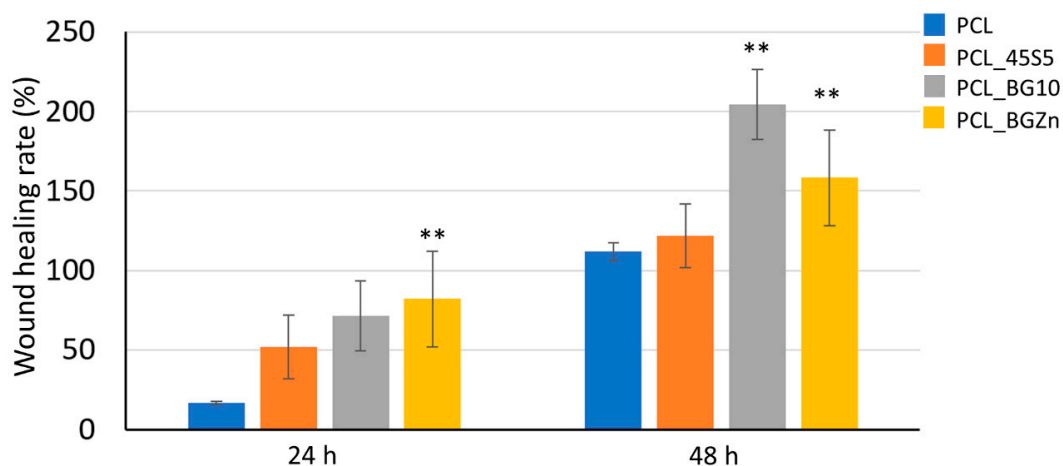


**Figure 9.** Wound-healing rate % (measured as cell migration rate %) 24 h and 48 h after the introduction of the “scratch” in confluent monolayers of NIH 3T3 cells in contact with eluates of PCL, PCL\_45S5, PCL\_BG10, and PCL\_BGZn composite electrospun mats. \*\*  $p < 0.05$ .

#### 4. Conclusions

PCL electrospun mats and composite electrospun mats suitable for wound-healing applications were successfully fabricated by electrospinning. Bioactive glasses with different compositions were embedded into a PCL matrix to enhance the cell response to the fiber mats. In fact, it is well-known that bioactive glass particles improve bioactivity, cell adhesion, and proliferation in composite, showing their suitability for applications in soft tissue engineering, as wound healing. Our results showed that both bioactivity and cell viability on composite fibers were higher compared to those of neat PCL electrospun mats, even though the amount of added bioactive glass was relatively low (5% wt with respect to PCL). In particular, the presence of BG does not inhibit cell viability, which was higher (for 45S5 and BGMS10) or comparable (for BGMS\_2Zn) with respect to neat PCL fibers. Furthermore, PCL/bioactive glass electrospun mats showed higher wound-healing rate (measured as cell migration rate) compared to neat PCL 48 h after the scratch *in vitro*. The incorporation of BGs and, in particular, the incorporation of BGMS10 achieved enhanced cell viability preserving the mechanical properties. Further work will be focused on the incorporation of a higher amount of bioactive glass particles and on investigating possible antimicrobial effects due to Zn ions.

**Author Contributions:** Investigation, writing—original draft preparation, R.S.; conceptualization, investigation, writing—review and editing, supervision, L.L.; conceptualization, writing—review and editing, supervision, V.C. and A.R.B. All authors have read and agreed to the published version of the manuscript.

**Funding:** This research received no external funding.

**Conflicts of Interest:** The authors declare no conflict of interest.

#### References

1. Jiang, T.; Carbone, E.J.; Lo, K.W.-H.; Laurencin, C.T. Electrospinning of polymer nanofibers for tissue regeneration. *Prog. Polym. Sci.* **2015**, *46*, 1–24. [[CrossRef](#)]
2. Loh, Q.L.; Choong, C. Three-dimensional scaffolds for tissue engineering applications: Role of porosity and pore size. *Tissue Eng. Part B Rev.* **2013**, *19*, 485–502. [[CrossRef](#)]
3. Rezwani, K.; Chen, Q.; Blaker, J.J.; Boccaccini, A.R. Biodegradable and bioactive porous polymer/inorganic composite scaffolds for bone tissue engineering. *Biomaterials* **2006**, *27*, 3413–3431. [[CrossRef](#)] [[PubMed](#)]
4. Sun, B.; Long, Y.-Z.; Zhang, H.; Li, M.; Duvail, J.; Jiang, X.; Yin, H. Advances in three-dimensional nanofibrous macrostructures via electrospinning. *Prog. Polym. Sci.* **2014**, *39*, 862–890. [[CrossRef](#)]
5. Shenoy, S.L.; Bates, W.D.; Frisch, H.L.; Wnek, G.E. Role of chain entanglements on fiber formation during electrospinning of polymer solutions: Good solvent, non-specific polymer-polymer interaction limit. *Polymer* **2005**, *46*, 3372–3384. [[CrossRef](#)]
6. Jarusuwannapoom, T.; Hongrojjanawiwat, W.; Jitjaicham, S.; Wannatong, L.; Nithitanakul, M.; Pattamaprom, C.; Koombhongse, P.; Rangkupan, R.; Supaphol, P. Effect of solvents on electro-spinnability of polystyrene solutions and morphological appearance of resulting electrospun polystyrene fibers. *Eur. Polym. J.* **2005**, *41*, 409–421. [[CrossRef](#)]
7. Van Der Schueren, L.; De Schoenmaker, B.; KalaogluÖzlem, I.; De Clerck, K. An alternative solvent system for the steady state electrospinning of polycaprolactone. *Eur. Polym. J.* **2011**, *47*, 1256–1263. [[CrossRef](#)]
8. Liverani, L.; Lacina, J.; Roether, J.A.; Boccardi, E.; Killian, M.S.; Schmuki, P.; Schubert, D.W.; Boccaccini, A.R. Incorporation of bioactive glass nanoparticles in electrospun PCL/chitosan fibers by using benign solvents. *Bioact. Mater.* **2018**, *3*, 55–63. [[CrossRef](#)]
9. Liverani, L.; Boccaccini, A. Versatile Production of Poly(Epsilon-Caprolactone) Fibers by Electrospinning Using Benign Solvents. *Nanomaterials* **2016**, *6*, 75. [[CrossRef](#)]
10. Liverani, L.; Killian, M.S.; Boccaccini, A.R. Fibronectin Functionalized Electrospun Fibers by Using Benign Solvents: Best Way to Achieve Effective Functionalization. *Front. Bioeng. Biotechnol.* **2019**, *7*, 1–12. Available online: <https://www.frontiersin.org/article/10.3389/fbioe.2019.00068/full> (accessed on 4 August 2020). [[CrossRef](#)]

11. Dziadek, M.; Pawlik, J.; Menaszek, E.; Ewa, S.-Z.; Cholewa-Kowalska, K. Effect of the preparation methods on architecture, crystallinity, hydrolytic degradation, bioactivity, and biocompatibility of PCL/bioglass composite scaffolds. *J. Biomed. Mater. Res. Part B Appl. Biomater.* **2015**, *103*, 1580–1593. [[CrossRef](#)] [[PubMed](#)]
12. Da Silva, G.R.; Lima, T.H.; Oréfice, R.L.; Silva-Cunha, A.; Silva-Cunha, A.; Zhao, M.; Behar-Cohen, F. In vitro and in vivo ocular biocompatibility of electrospun poly( $\epsilon$ -caprolactone) nanofibers. *Eur. J. Pharm. Sci.* **2015**, *73*, 9–19. [[CrossRef](#)] [[PubMed](#)]
13. Lee, K.; Kim, H.Y.; Khil, M.; Ra, Y.; Lee, D. Characterization of nano-structured poly( $\epsilon$ -caprolactone) nonwoven mats via electrospinning. *Polymer* **2003**, *44*, 1287–1294. [[CrossRef](#)]
14. Rahaman, M.N.; Day, D.E.; Bal, B.S.; Fu, Q.; Jung, S.B.; Bonewald, L.F.; Tomsia, A.P. Bioactive glass in tissue engineering. *Acta Biomater.* **2011**, *7*, 2355–2373. [[CrossRef](#)] [[PubMed](#)]
15. Jones, J.R.; Brauer, D.S.; Hupa, L.; Greenspan, D.C. Bioglass and Bioactive Glasses and Their Impact on Healthcare. *Int. J. Appl. Glas. Sci.* **2016**, *7*, 423–434. [[CrossRef](#)]
16. Hench, L.L.; Splinter, R.J.; Allen, W.C.; Greenlee, T.K. Bonding Mechanisms at the Interface of Ceramic Prosthetic Materials. *J. Biomed. Mater. Res.* **1971**, *2*, 117–141. [[CrossRef](#)]
17. Bellucci, D.; Cannillo, V. A novel bioactive glass containing strontium and magnesium with ultra-high crystallization temperature. *Mater. Lett.* **2018**, *213*, 67–70. [[CrossRef](#)]
18. Bellucci, D.; Salvatori, R.; Anesi, A.; Chiarini, L.; Cannillo, V. SBF assays, direct and indirect cell culture tests to evaluate the biological performance of bioglasses and bioglass-based composites: Three paradigmatic cases. *Mater. Sci. Eng. C* **2019**, *96*, 757–764. [[CrossRef](#)]
19. Bellucci, D.; Salvatori, R.; Giannatiempo, J.; Anesi, A.; Bortolini, S.; Cannillo, V. A New Bioactive Glass / Collagen Hybrid Composite for Applications in Dentistry. *Materials* **2019**, *12*, 2079. [[CrossRef](#)]
20. Bellucci, D.; Veronesi, E.; Strusi, V.; Petrachi, T.; Murgia, A.; Mastrolia, I.; Dominici, M.; Cannillo, V. Human Mesenchymal Stem Cell Combined with a New Strontium-Enriched Bioactive Glass: An ex-vivo Model for Bone Regeneration. *Materials* **2019**, *12*, 3633. [[CrossRef](#)]
21. Bellucci, D.; Veronesi, E.; Dominici, M.; Cannillo, V. On the in vitro biocompatibility testing of bioactive glasses. *Materials* **2020**, *13*, 1816. [[CrossRef](#)] [[PubMed](#)]
22. Elsayed, H.; Romero, A.R.; Bellucci, D.; Cannillo, V.; Bernardo, E. Advanced open-celled structures from low-temperature sintering of a crystallization-resistant bioactive glass. *Materials* **2019**, *12*, 3653. [[CrossRef](#)] [[PubMed](#)]
23. Sergi, R.; Bellucci, D.; Salvatori, R.; Cannillo, V. Chitosan based bioactive glass gauze: Microstructural properties, in vitro bioactivity and biological tests. *Materials* **2020**, *13*, 2819. [[CrossRef](#)] [[PubMed](#)]
24. Sergi, R.; Bellucci, D.; Salvatori, R.; Maisetta, G.; Batoni, G.; Cannillo, V. Zinc containing bioactive glasses with ultra-high crystallization temperature, good biological performance and antibacterial effects. *Mater. Sci. Eng. C* **2019**, *104*, 109910. [[CrossRef](#)]
25. Xynos, I.D.; Edgar, A.J.; Buttery, L.D.; Hench, L.L.; Polak, J.M. Ionic products of bioactive glass dissolution increase proliferation of human osteoblasts and induce insulin-like growth factor II mRNA expression and protein synthesis. *Biochem. Biophys. Res. Commun.* **2000**, *276*, 461–465. [[CrossRef](#)] [[PubMed](#)]
26. O'Neill, E.; Awale, G.; Daneshmandi, L.; Umerah, O.; Lo, K.W.-H. The roles of ions on bone regeneration. *Drug Discov. Today* **2018**, *23*, 879–890. [[CrossRef](#)]
27. Valerio, P.; Pereira, M.M.; Goes, A.M.; Leite, M. The effect of ionic products from bioactive glass dissolution on osteoblast proliferation and collagen production. *Biomaterials* **2004**, *25*, 2941–2948. [[CrossRef](#)]
28. Baino, F.; Hamzehlou, S.; Kargozar, S. Bioactive Glasses: Where Are We and Where Are We Going? *J. Funct. Biomater.* **2018**, *9*, 25. [[CrossRef](#)]
29. Yang, F.; Yang, D.; Tu, J.; Zheng, Q.; Cai, L.; Wang, L. Strontium enhances osteogenic differentiation of mesenchymal stem cells and in vivo bone formation by activating Wnt/catenin signaling. *Stem Cells* **2011**, *29*, 981–991. [[CrossRef](#)]
30. Bonnelye, E.; Chabadel, A.; Saltel, F.; Jurdic, P. Dual effect of strontium ranelate: Stimulation of osteoblast differentiation and inhibition of osteoclast formation and resorption in vitro. *Bone* **2008**, *42*, 129–138. [[CrossRef](#)]
31. Mao, L.; Xia, L.; Chang, J.; Liu, J.; Jiang, L.; Wu, C.; Fang, B. The synergistic effects of Sr and Si bioactive ions on osteogenesis, osteoclastogenesis and angiogenesis for osteoporotic bone regeneration. *Acta Biomater.* **2017**, *61*, 217–232. [[CrossRef](#)] [[PubMed](#)]

32. Weng, L.; Chandorkar, Y.; Teusink, M.J.; Shuler, F.D.; Li, X.; Xie, J. Binary Doping of Strontium and Copper Enhancing Osteogenesis and Angiogenesis of Bioactive Glass Nanofibers while Suppressing Osteoclast Activity. *ACS Appl. Mater. Interfaces* **2017**, *9*, 24484–24496. [CrossRef] [PubMed]
33. Zhang, Y.; Cui, X.; Zhao, S.; Wang, H.; Rahaman, M.N.; Liu, Z.; Huang, W.; Zhang, C. Evaluation of injectable strontium-containing borate bioactive glass cement with enhanced osteogenic capacity in a critical-sized rabbit femoral condyle defect model. *ACS Appl. Mater. Interfaces* **2015**, *7*, 2393–2403. [CrossRef] [PubMed]
34. Gorustovich, A.; Roether, J.A.; Boccaccini, A.R. Effect of Bioactive Glasses on Angiogenesis: A Review of *In Vitro* and *In Vivo* Evidences. *Tissue Eng. Part B Rev.* **2010**, *16*, 199–207. [CrossRef] [PubMed]
35. Yu, H.; Peng, J.; Xu, Y.; Chang, J.; Li, H. Bioglass Activated Skin Tissue Engineering Constructs for Wound Healing. *ACS Appl. Mater. Interfaces* **2016**, *8*, 703–715. [CrossRef] [PubMed]
36. Baino, F.; Novajra, G.; Miguez-Pacheco, V.; Boccaccini, A.R.; Vitale-Brovarone, C. Bioactive glasses: Special applications outside the skeletal system. *J. Non Cryst. Solids* **2016**, *432*, 15–30. [CrossRef]
37. Reginster, J.Y.; Badurski, J.; Bellamy, N.; Bensen, W.; Chapurlat, R.; Chevalier, X.; Christiansen, C.; Genant, H.; Navarro, F.; Nasonov, E.; et al. Efficacy and safety of strontium ranelate in the treatment of knee osteoarthritis: Results of a double-blind, randomised placebo-controlled trial. *Ann. Rheum. Dis.* **2013**, *72*, 179–186. [CrossRef]
38. Dasgupta, S.; Banerjee, S.S.; Bandyopadhyay, A.; Bose, S. Zn-and Mg-Doped Hydroxyapatite Nanoparticles for Controlled Release of Protein. *Langmuir* **2010**, *26*, 4958–4964. [CrossRef]
39. Lijuan, X.; Liyun, J.; Lixin, J.; Chengdong, X. Synthesis of Mg-substituted hydroxyapatite nanopowders: Effect of two different magnesium sources. *Mater. Lett.* **2013**, *106*, 246–249. [CrossRef]
40. Cacciotti, I. Bivalent cationic ions doped bioactive glasses: The influence of magnesium, zinc, strontium and copper on the physical and biological properties. *J. Mater. Sci.* **2017**, *52*, 8812–8831. [CrossRef]
41. MacDonald, R. The role of Zinc in Growth and Cell Proliferation. *J. Nutr.* **2000**, *130*, 1488–1492. Available online: <http://jn.nutrition.org/content/130/5/1447S.long> (accessed on 4 August 2020). [CrossRef] [PubMed]
42. Maret, W. Zinc in Cellular Regulation: The Nature and Significance of “Zinc Signals”. *Int. J. Mol. Sci.* **2017**, *18*, 2285. [CrossRef] [PubMed]
43. Huang, M.; Hill, R.G.; Rawlinson, S. Zinc bioglasses regulate mineralization in human dental pulp stem cells. *Dent. Mater.* **2017**, *33*, 543–552. [CrossRef] [PubMed]
44. Pasquet, J.; Chevalier, Y.; Couval, E.; Bouvier, D.; Noizet, G.; Morlière, C.; Bolzinger, M.-A. Antimicrobial activity of zinc oxide particles on five micro-organisms of the Challenge Tests related to their physicochemical properties. *Int. J. Pharm.* **2014**, *460*, 92–100. [CrossRef] [PubMed]
45. Kamitakahara, M.; Ohtsuki, C.; Inada, H.; Tanihara, M.; Miyazaki, T. Effect of ZnO addition on bioactive CaO-SiO<sub>2</sub>-P<sub>2</sub>O<sub>5</sub>-CaF<sub>2</sub> glass-ceramics containing apatite and wollastonite. *Acta Biomater.* **2006**, *2*, 467–471. [CrossRef]
46. Pasquet, J.; Chevalier, Y.; Couval, E.; Bouvier, D.; Bolzinger, M.-A. Zinc oxide as a new antimicrobial preservative of topical products: Interactions with common formulation ingredients. *Int. J. Pharm.* **2015**, *479*, 88–95. [CrossRef]
47. Miguez-Pacheco, V.; Gorustovich, A.; Roether, J.A.; Boccaccini, A.R. Bioactive glasses for soft tissue engineering applications. In *Bioactive Glasses: Fundamentals, Technology and Applications* Royal Society of Chemistry; Royal Society of Chemistry: Cambridge, UK, 2017; pp. 336–361.
48. Saghiri, M.A.; Asatourian, A.; Orangi, J.; Sorenson, C.M.; Sheibani, N. Functional role of inorganic trace elements in angiogenesis—Part II: Cr, Si, Zn, Cu, and S. *Crit. Rev. Oncol. Hematol.* **2015**, *96*, 143–155. [CrossRef]
49. Kargozar, S.; Baino, F.; Hamzehlou, S.; Hill, R.G.; Mozafari, M. Bioactive Glasses: Sprouting Angiogenesis in Tissue Engineering. *Trends Biotechnol.* **2018**, *36*, 430–444. [CrossRef]
50. Gaharwar, A.; Nikkhah, M.; Sant, S.; Khademhosseini, A. Anisotropic Poly (glycerol sebacate)-Poly ( $\epsilon$ -caprolactone) Electrospun Fibers Promote Endothelial Cell Guidance. *Biofabrication* **2016**, *7*, 1–19.
51. Bellucci, D.; Cannillo, V.; Ciardelli, G.; Gentile, P.; Sola, A. Potassium based bioactive glass for bone tissue engineering. *Ceram. Int.* **2010**, *36*, 2449–2453. [CrossRef]
52. Bellucci, D.; Cannillo, V.; Sola, A. A new potassium-based bioactive glass: Sintering behaviour and possible applications for bioceramic scaffolds. *Ceram. Int.* **2011**, *37*, 145–157. [CrossRef]
53. Bellucci, D.; Cannillo, V.; Sola, A. Calcium and potassium addition to facilitate the sintering of bioactive glasses. *Mater. Lett.* **2011**, *65*, 1825–1827. [CrossRef]

54. Caroline, A.; Schneider Wayne, S. Rasband and KWE. *Image J. Fundam. Digit. Imaging Med.* **2010**, *9*, 185–188.
55. Shahin-Shamsabadi, A.; Hashemi, A.; Tahriri, M.; Bastami, F.; Salehi, M.; Abbas, F.M. Mechanical, material, and biological study of a PCL/bioactive glass bone scaffold: Importance of viscoelasticity. *Mater. Sci. Eng. C* **2018**, *90*, 280–288. [[CrossRef](#)]
56. Maçon, A.L.B.; Kim, T.B.; Valliant, E.M.; Goetschius, K.; Brow, R.K.; Day, D.E. A unified in vitro evaluation for apatite-forming ability of bioactive glasses and their variants of bioactive glasses and their variants. *J. Mater. Sci. Mater. Med.* **2015**, *26*, 115. Available online: [https://spiral.imperial.ac.uk/bitstream/10044/1/26039/2/TC04\\_RR\\_Paper\\_forspiral](https://spiral.imperial.ac.uk/bitstream/10044/1/26039/2/TC04_RR_Paper_forspiral) (accessed on 4 August 2020).
57. Kokubo, T.; Takadama, H. How useful is SBF in predicting in vivo bone bioactivity? *Biomaterials* **2006**, *27*, 2907–2915. [[CrossRef](#)]
58. Yamaguchi, A.; Hirose, S. Characterization of osteoblastic differentiation of stromal cell line ST2 that is induced by ascorbic acid. *Am. J. Physiol.* **1999**, *277*, C132–C138.
59. Robins, J.C.; Akeno, N.; Mukherjee, A.; Dalal, R.R.; Aronow, B.J.; Koopman, P.; Clemens, T.L. Hypoxia induces chondrocyte-specific gene expression in mesenchymal cells in association with transcriptional activation of Sox9. *Bone* **2005**, *37*, 313–322. [[CrossRef](#)]
60. Ding, J.; Nagai, K.; Woo, J. Insulin-Dependent Adipogenesis in Stromal ST2 Cells Derived from Murine Bone Marrow. *Biosci. Biotechnol. Biochem.* **2003**, *67*, 314–321. [[CrossRef](#)]
61. Liverani, L.; Boccardi, E.; Beltrán, A.; Boccaccini, A.R. Incorporation of calcium containing mesoporous (MCM-41-type) particles in electrospun PCL fibers by using benign solvents. *Polymers* **2017**, *9*, 487. [[CrossRef](#)]
62. Todaro, G.J.; Lazar, G.K.; Green, H. The initiation of cell division in a contact-inhibited mammalian cell line. *J. Cell. Comp. Physiol.* **1965**, *66*, 325–333. [[CrossRef](#)] [[PubMed](#)]
63. Jonkman, J.E.N.; Cathcart, J.A.; Xu, F.; Bartolini, M.E.; Amon, J.E.; Stevens, K.M.; Colarusso, P. An introduction to the wound healing assay using live-cell microscopy. *Cell Adhes. Migr.* **2014**, *8*, 440–451. [[CrossRef](#)] [[PubMed](#)]
64. Grada, A.; Otero-Viñas, M.; Prieto-Castrillo, F.; Obagi, Z.; Falanga, V. Research Techniques Made Simple: Analysis of Collective Cell Migration Using the Wound Healing Assay. *J. Investig. Dermatol.* **2017**, *137*, e11ee16. [[CrossRef](#)] [[PubMed](#)]
65. Ghasemi-mobarakeh, L.; Prabhakaran, M.P.; Morshed, M. Electrospun poly(3-caprolactone)/gelatin nanofibrous scaffolds for nerve tissue engineering. *Biomaterials* **2008**, *29*, 4532–4539. [[CrossRef](#)]
66. Qin, X.; Wu, D. Effect of different solvents on poly(caprolactone)(PCL) electrospun nonwoven membranes. *J. Therm. Anal. Calorim.* **2012**, *107*, 1007–1013. [[CrossRef](#)]
67. Gautam, S.; Dinda, A.K.; Mishra, N.C. Fabrication and characterization of PCL/gelatin composite nanofibrous scaffold for tissue engineering applications by electrospinning method. *Mater. Sci. Eng. C* **2013**, *33*, 1228–1235. [[CrossRef](#)]
68. Correia, C.; Leite, Á.J.; Mano, J.F. Chitosan/bioactive glass nanoparticles scaffolds with shape 511 memory properties. *Carbohydr. Polym.* **2015**, *123*, 39–45. [[CrossRef](#)]
69. Ratner, B.; Hoffman, A.; Schoen, F.; Lemons, J. An Introduction to Materials in Medicine 2nd Edition. *Biomater. Sci.* **2004**, *484*, 1–851.
70. Cipitria, A.; Skelton, A.; Dargaville, T.R.; Dalton, P.D.; Hutmacher, D.W. Design, fabrication and characterization of PCL electrospun scaffolds—A review. *J. Mater. Chem.* **2011**, *21*, 9419–9453. [[CrossRef](#)]
71. Wan, Y.; Lu, X.; Dalai, S.; Zhang, J. Thermophysical properties of polycaprolactone/chitosan blend membranes. *Thermochim. Acta* **2009**, *487*, 33–38. [[CrossRef](#)]
72. Ma, W.; Yang, X.; Ma, L.; Wang, X.; Zhang, L.; Yang, G.; Han, C.; Gou, Z. Fabrication of bioactive glass-introduced nanofibrous membranes with multifunctions for potential wound dressing. *RSC Adv.* **2014**, *4*, 60114–60122. [[CrossRef](#)]
73. Naseri, S.; Lepry, W.C.; Nazhat, S.N. Bioactive glasses in wound healing: Hope or hype? *J. Mater. Chem. B* **2017**, *5*, 6167–6174. [[CrossRef](#)] [[PubMed](#)]
74. Luz, G.M.; Mano, J.F. Chitosan/bioactive glass nanoparticles composites for biomedical applications. *Biomed. Mater.* **2012**, *7*, 054104. [[CrossRef](#)] [[PubMed](#)]
75. Luz, G.; Boesel, L.; Del Campo, A.; Mano, J.F. Micropatterning of bioactive glass nanoparticles on chitosan membranes for spatial controlled biomineralization. *Langmuir* **2012**, *28*, 6970–6977. [[CrossRef](#)]

76. Zheng, K.; Solodovnyk, A.; Li, W.; Goudouri, O.-M.; Stähli, C.; Nazhat, S.N.; Boccaccini, A.R. Aging time and temperature effects on the structure and bioactivity of gel-derived 45S5 glass-ceramics. *J. Am. Ceram. Soc.* **2015**, *98*, 30–38. [[CrossRef](#)]
77. Aguiar, H.; Serra, J.; González, P.; León, B. Structural study of sol-gel silicate glasses by IR and Raman spectroscopies. *J. Non Cryst. Solids* **2009**, *355*, 475–480. [[CrossRef](#)]
78. Mohini, G.J.; Krishnamacharyulu, N.; Baskaran, G.S.; Rao, P.V.; Veeraiah, N.; Nalluri, V. Studies on influence of aluminium ions on the bioactivity of B<sub>2</sub>O<sub>3</sub>-SiO<sub>2</sub>-P<sub>2</sub>O<sub>5</sub>-Na<sub>2</sub>O-CaO glass system by means of spectroscopic studies. *Appl. Surf. Sci.* **2013**, *287*, 46–53. [[CrossRef](#)]
79. Lázaro, G.S.; Santos, S.C.; Resende, C.X.; Dos Santos, E.A. Individual and combined effects of the elements Zn, Mg and Sr on the surface reactivity of a SiO<sub>2</sub>-CaO-Na<sub>2</sub>O-P<sub>2</sub>O<sub>5</sub> bioglass system. *J. Non Cryst. Solids* **2014**, *386*, 19–28. [[CrossRef](#)]
80. Rabiee, S.M.; Nazparvar, N.; Azizian, M.; Vashae, D.; Tayebi, L. Effect of ion substitution on properties of bioactive glasses: A review. *Ceram. Int.* **2015**, *41*, 7241–7251. [[CrossRef](#)]
81. Aina, V.; Malavasi, G.; Pla, A.F.; Munaron, L.; Morterra, C. Zinc-containing bioactive glasses: Surface reactivity and behaviour towards endothelial cells. *Acta Biomater* **2009**, *5*, 1211–1222. [[CrossRef](#)]
82. Wajda, A.; Goldmann, W.H.; Detsch, R.; Boccaccini, A.R.; Sitarz, M. Influence of zinc ions on structure, bioactivity, biocompatibility and antibacterial potential of melt-derived and gel-derived glasses from CaO-SiO<sub>2</sub> system. *J. Non Cryst. Solids* **2019**, *511*, 86–99. [[CrossRef](#)]
83. Haimi, S.; Gorianc, G.; Moimas, L.; Lindroos, B.; Huhtala, H.; Rätty, S.; Kuokkanen, H.; Sándor, G.K.; Schmid, C.; Miettinen, S. Characterization of zinc-releasing three-dimensional bioactive glass scaffolds and their effect on human adipose stem cell proliferation and osteogenic differentiation. *Acta Biomater.* **2009**, *5*, 3122–3131. [[CrossRef](#)] [[PubMed](#)]
84. Jell, G.; Notingher, P.; Tsigkou, O.; Polak, J.; Hench, L.; Stevens, M.M.; Notingher, I. Bioactive glass-induced osteoblast differentiation: A noninvasive spectroscopic study. *J. Biomed. Mater. Res.* **2008**, *86A*, 31–40. [[CrossRef](#)] [[PubMed](#)]
85. Zhao, F.; Zhang, W.; Fu, X.; Xie, W.; Chen, X. Fabrication and characterization of bioactive glass/alginate composite scaffolds by a self-crosslinking processing for bone regeneration. *RSC Adv.* **2016**, *6*, 91201–91208. [[CrossRef](#)]
86. Aina, V.; Perardi, A.; Bergandi, L.; Malavasi, G.; Menabue, L.; Morterra, C.; Ghigo, D. Cytotoxicity of zinc-containing bioactive glasses in contact with human osteoblasts. *Chem. Biol. Interact.* **2007**, *167*, 207–218. [[CrossRef](#)]
87. Ito, A.; Ojima, K.; Naito, H.; Ichinose, N.; Tateishi, T. Preparation, solubility, and cytocompatibility of zinc-releasing calcium phosphate ceramics. *J. Biomed. Mater. Res.* **2000**, *50*, 178–183. [[CrossRef](#)]
88. Gentleman, E.; Fredholm, Y.C.; Jell, G.; Lotfibakhshaiesh, N.; O'Donnell, M.; Hill, R.G.; Stevens, M.M. The effects of strontium-substituted bioactive glasses on osteoblasts and osteoclasts in vitro. *Biomaterials* **2010**, *31*, 3949–3956. [[CrossRef](#)]
89. O'Donnell, M.; Hill, R. Influence of strontium and the importance of glass chemistry and structure when designing bioactive glasses for bone regeneration. *Acta Biomater.* **2010**, *6*, 2382–2385. Available online: <http://www.ncbi.nlm.nih.gov/pubmed/20079468> (accessed on 4 August 2020). [[CrossRef](#)]
90. Massera, J.; Kokkari, A.; Närhi, T.; Hupa, L. The influence of SrO and CaO in silicate and phosphate bioactive glasses on human gingival fibroblasts. *J. Mater. Sci. Mater. Med.* **2015**, *26*, 196. [[CrossRef](#)]
91. Liang, C.-C.; Park, A.Y.; Guan, J.-L. In vitro scratch assay: A convenient and inexpensive method for analysis of cell migration in vitro. *Nat. Protoc.* **2007**, *2*, 329–333. [[CrossRef](#)]
92. Badr-Mohammadi, M.-R.; Hesaraki, S.; Zamanian, A. Mechanical properties and in vitro cellular behavior of zinc-containing nano-bioactive glass doped biphasic calcium phosphate bone substitutes. *J. Mater. Sci. Mater. Med.* **2014**, *25*, 185–197. [[CrossRef](#)] [[PubMed](#)]
93. Jones, J.R. Reprint of: Review of bioactive glass: From Hench to hybrids. *Acta Biomater.* **2015**, *23*, S53–S82. [[CrossRef](#)] [[PubMed](#)]
94. Hench, L.L. The story of Bioglass®. *J. Mater. Sci. Mater. Med.* **2006**, *17*, 967–978. [[CrossRef](#)] [[PubMed](#)]
95. Putney, J.W. *Calcium Signaling*, 2nd ed.; CRC Press: Boca Raton, FL, USA, 2005; pp. 1–540.
96. Humeau, J.; Pedro, J.M.B.-S.; Vitale, I.; Nuñez, L.; Villalobos, C.; Kroemer, G.; Senovilla, L. Calcium signaling and cell cycle: Progression or death. *Cell Calcium.* **2018**, *70*, 3–15. [[CrossRef](#)] [[PubMed](#)]

97. Maret, W. Metals on the move: Zinc ions in cellular regulation and in the coordination dynamics of zinc proteins. *BioMetals* **2011**, *24*, 411–418. [[CrossRef](#)]
98. Maywald, M.; Wessels, I.; Rink, L. Zinc signals and immunity. *Int. J. Mol. Sci.* **2017**, *18*, 2222. [[CrossRef](#)]
99. Jia, L.; Yiyuan, K.; Wei, Z.; Limin, W.; Liangjiao, C.; Bin, S.; Shao, L. Ion-Shedding Zinc Oxide Nanoparticles Induce Microglial BV2 Cell Proliferation via the ERK and Akt Signaling Pathways. *Toxicol. Sci.* **2017**, *156*, 167–178. [[CrossRef](#)]
100. Hasan, R.; Rink, L.; Haase, H. Zinc signals in neutrophil granulocytes are required for the formation of neutrophil extracellular traps. *Innate Immun.* **2013**, *19*, 253–264. [[CrossRef](#)]



© 2020 by the authors. Licensee MDPI, Basel, Switzerland. This article is an open access article distributed under the terms and conditions of the Creative Commons Attribution (CC BY) license (<http://creativecommons.org/licenses/by/4.0/>).